The Extended Vienna System-Level Simulator for Reconfigurable Intelligent Surfaces

Le Hao[1], Stefan Schwarz[1,2], Markus Rupp[1]
[1] Institute of Telecommunications, Technische Universität (TU) Wien
[2] Christian Doppler Laboratory for Dependable Wireless Connectivity for the Society in Motion
Gusshausstrasse 25, 1040 Vienna, Austria
le.hao@tuwien.ac.at, stefan.schwarz@tuwien.ac.at, markus.rupp@tuwien.ac.at

***Abstract*—Reconfigurable intelligent surfaces (RISs) have been considered a promising research direction for the next generation of wireless communications. It is essential to perform extensive simulations in a system-level simulator (SLS) to analyze the system performance of RIS-assisted large-scale wireless networks. This paper introduces the RIS-tailored Vienna SLS that utilizes the MATLAB ray tracer to realize RIS-assisted transmissions. A recently published free space pathloss model for RIS (RISFSPL) has been adopted to be compatible with our SLS. In addition, we modified the ray tracing (RT) model based on the RISFSPL model to obtain a more precise pathloss in a realistic environment. In this way, we realize the advantages of both the RISFSPL and RT models. We verified the system performance through simulations in a single-input single-output (SISO) scenario with random and optimized RIS phase shifts. Furthermore, we analyzed the system performance through simulations in a complex scenario that consists of multiple base stations (BSs), RISs, and users.**

***Keywords*—Reconfigurable Intelligent Surface (RIS); Intelligent Reflecting Surface (IRS); System level simulation; 6G**

I. Introduction

Reconfigurable intelligent surfaces (RISs) have been considered an attractive technology for the next generation of wireless communications [1]. RIS is an artificial planar structure that consists of many elements with reconfigurable properties. Properly tuning the RIS phase shifts can steer the impinging signals in desired directions and achieve constructive or destructive combinations of signals [2]. RIS can be used to enhance the received signal strength, increase energy efficiency, and compensate for blind zones [3]. It is low cost, easy to install on building facades or ceilings, and compatible with existing and future wireless systems due to its nearly passive structure [4].

In recent years, academia and industry have conducted intensive research on RIS-assisted wireless systems. The authors in [5] give an overview of intelligent radio environments, including a RIS design from the electromagnetic wave aspect and communication aspect, different functions to describe the RIS behavior, and the advantages and limitations when applying RIS. In [6], the authors compare the most frequently used communication models for RIS-based wireless communication systems to evaluate and optimize the system performance. The authors in [7] develop a power consumption model for a RIS-based downlink multi-user multiple-input-single-output (MU MISO) system to improve energy efficiency.

However, most research has been descriptive in electrical and magnetic field analysis and focused on link-level evaluation. Even though some researchers have fabricated RIS and carried out measurements with RIS [8], this can only be conducted at a small-scale link level. A potent simulation tool is desperately needed to fill the gap left by system-level simulation and network performance evaluation. In paper [9], the authors perform system-level simulations for a RIS-assisted urban city scenario and analyze the performance advantages. To the author's best knowledge, however, there is yet no fully developed open-access SLS available that supports RIS-assisted large-scale wireless systems.

This paper introduces an extension of the well-established open-source Vienna 5G SLS to support RIS-assisted transmissions in large-scale cellular networks. Interested readers can find details of the simulator in [10]. We adopt an existing pathloss model to make it compatible with our existing system-level modeling approach [11], and verify the simulation results. In addition, we use the modified pathloss model as a reference to implement a ray tracing (RT)-based pathloss model for simulating more realistic scenarios. After the performance is verified in a SISO scenario, we analyze the system performance in a complex scenario that contains multiple BSs, RISs, and users.

The remaining part of this paper is organized as follows. Section II describes the RIS module in the Vienna SLS, including a comparison of two different pathloss models. Section III verifies and compares simulation results from the two models in a SISO scenario. In Section IV, the system performance in a complex scenario is investigated through simulations. In the end, conclusions are drawn in Section V.

Notation: We use italic letters, bold-face lower-case, and upper-case letters to denote scalars, vectors, and matrices, respectively. The symbol $\mathbb{C}^{a\times b}$ indicates the space of $a \times b$ complex-valued matrices. The term $\arg(\cdot)$ represents the phase, and $\mathrm{diag}(\cdot)$ represents a square diagonal matrix. We use $\odot$ to denote the Hadamard product. The conjugate transpose of $\mathbf{x}$ is denoted as $\mathbf{x}^{\mathrm{H}}$. The symbols $|\cdot|$ and $\mathbb{E}(\cdot)$ stand for absolute and expected values, respectively.

II. RIS-tailored system-level simulator

At the current stage of RIS-related research activities, the modeling and optimization of RIS-assisted systems are usually

focused on small-scale networks, where only a couple of RISs are analyzed in a simple scenario. However, it is essential to perform extensive system-level simulations before a new technology carries into practice. For this issue, the RT tool (e.g., MATLAB ray tracer, Wireless InSite) and SLS play a vital role in simulating large-scale networks in a realistic environment [5].

A. RIS Free Space Pathloss (RISFSPL) Model

Since the Vienna SLS is an open-access tool, we have implemented a RIS module and included support for the MATLAB ray tracer in this simulator. A first implementation of RIS can be found in [12], including macroscopic fading, small-scale fading, RIS modeling, and RIS phase shift optimization in a SISO scenario. As this was not validated by measurements, we implemented now a pathloss model for RIS that has been proved by measurements [13]. Yet, a straightforward implementation of the RISFPSL within our simulator is not possible, as our simulator relies on explicitly modeling the channel between all pairs of antenna elements (including RIS antenna elements). However, the model of [13] represents the composite scattering attenuation of the entire RIS system, including the interaction of multiple RIS antenna elements. As a result, we needed to adapt this pathloss model for RIS to be compatible with the SLS.

We assume a RIS consisting of L elements. Based on the far-field approximation, the distance between the transmitter and each RIS element can be regarded as the same, which is denoted as d_t. The distance between each RIS element and the receiver is the same, which is denoted as d_r. Each RIS element has the same effective aperture A, and gain G. The mutual coupling effect between each RIS element is not considered in this paper. The reflection coefficient of the l-th RIS element is given by $\Gamma^{(l)} = \alpha^{(l)} e^{j\phi^{(l)}}$ with $l \in 1, ..., L$. The terms $\alpha^{(l)}$ and $\phi^{(l)}$ are the amplitude and phase shift of the l-th RIS element, respectively. In the ideal case, we assume that the RIS reflects all the signal power it receives, i.e., $\alpha^{(l)} = 1$. Hence, the reflected signal power from the l-th RIS element can be expressed by

$$P_{re}^{(l)} = P_i^{(l)} |\Gamma^{(l)}|^2 = P_i^{(l)}, \tag{1}$$

with $P_i^{(l)}$ the incident signal power from the BS to the l-th RIS element. According to Friis formula, $P_i^{(l)}$ can be obtained by

$$P_i^{(l)} = \frac{P_t G_t A}{4\pi (d_t)^2}, \tag{2}$$

where P_t and G_t are the transmit power and gain of the transmit antenna, respectively.

The received signal power at the user side from the l-th RIS element can be written as

$$P_r^{(l)} = \frac{P_{re}^{(l)} G A_r}{4\pi (d_r)^2}, \tag{3}$$

where A_r is the effective aperture of the receiving antenna and can be calculated as follows

$$A_r = \frac{G_r \lambda^2}{4\pi}, \tag{4}$$

with G_r the gain of the receiving antenna.

The overall received power at the user side from all the RIS elements can be expressed as [14]

$$P_r = \frac{|E_r|^2 A_r}{2Z_0}, \tag{5}$$

where Z_0 is the characteristic impedance of the air. The term E_r is the total electric field of the received signal at the user from the RIS, and it can be obtained by

$$E_r = \sum_{l=1}^{L} E_r^{(l)}, \tag{6}$$

where $E_r^{(l)}$ is the electric field from l-th RIS element and is calculated by

$$E_r^{(l)} = \sqrt{\frac{2Z_0 P_r^{(l)}}{A_r}} e^{-j\psi_r^{(l)}}. \tag{7}$$

Here $\psi_r^{(l)}$ is the phase alteration of the received signal caused by the signal propagation and the reflection coefficient of the l-th RIS element.

By combining (1), (2), (3), (6) and (7), we obtain

$$E_r = \sqrt{\frac{Z_0 P_t G_t G A}{8\pi^2 (d_t d_r)^2}} \sum_{l=1}^{L} e^{-j\psi_r^{(l)}}. \tag{8}$$

By combining (4) and (5), we get

$$P_r = \frac{|E_r|^2 G_r \lambda^2}{8\pi Z_0}. \tag{9}$$

The SLS uses the average received signal power obtained from (9) for cell assignment. We assign the BS that leads to the maximum received power or maximum signal to interference and noise ratio (SINR) as the desired BS for the user, and other BSs are regarded as interfering BSs. During this phase, the RIS phases cannot be optimized for a user as the user is not yet attached to the BS. Therefore, this received power should be based on random RIS phases. We replace $|E_r|^2$ by its expected value, with expectation taken over the phases $\psi_r^{(l)}$. To calculate this expected value, we assume that $\psi_r^{(l)}$ are uniform random in $[0, 2\pi]$ and statistically independent. As a result, we can rewrite (9) by inserting (8) as

$$P_r = \frac{P_t G_t G G_r \lambda^2 A}{64\pi^3 (d_t d_r)^2} \sum_{l=1}^{L} \left| e^{-j\psi_r^{(l)}} \right|^2 = \frac{P_t G_t G G_r \lambda^2 L A}{64\pi^3 (d_t d_r)^2}. \tag{10}$$

Yet, as soon as a user is connected to a BS, we can optimize the RIS phases for this user. The main difference between our pathloss model and the pathloss model from [13] is that they assume the RIS phases are already optimized for the user when calculating the pathloss, and hence, the phasor in (9) is summed coherently in [13]. In their approach, the RIS phase shift optimization happens purely in macroscopic fading, no small-scale fading is involved. The direct link is not considered in that paper, either. However, in the SLS, we need to include all the direct and RIS-assisted links, as well as the macroscopic

fading and small-scale fading. We optimize the RIS phase shifts according to the channel information of each link, and hence, the RIS phase shift optimization is done in small-scale fading.

The RIS phase shift optimization in the SLS only supports the SISO scenario in the current state. We assume a single-antenna BS and a single-antenna user with a RIS consisting of L elements. We use h_d, $\mathbf{h}_t \in \mathbb{C}^{1\times L}$ and $\mathbf{h}_r \in \mathbb{C}^{1\times L}$ to denote the small-scale fading of BS-user, BS-RIS, and RIS-user links, respectively. We assume the BS-RIS and RIS-UE links have strong line-of-sight (LOS) paths. Therefore, $\mathbf{h}_t$ and $\mathbf{h}_r$ are generated based on the Rician model, and h_d is generated according to the Rayleigh channel model. The average power of h_d, $\mathbf{h}_t$ and $\mathbf{h}_r$ are all normalized to one, i.e., $\mathbb{E}(|h_d|^2) = 1$, etc. According to [15], the optimized phase shift of the l-th RIS element is calculated as $\phi^{(l)} = \arg(h_d) - \arg(\mathbf{h}_t^{(l)} \odot \mathbf{h}_r^{(l)})$.

The user receives signals from both the direct link and the RIS-assisted link. Let $\text{MF}_{\text{d,RISFSPL}}$ and $\text{MF}_{\text{ris,RISFSPL}}$ denote the macroscopic fading of the direct link and RIS-link, respectively. In the SLS, we assume the gain of RIS and user antenna equal to one as default, i.e., $G = G_r = 1$. According to (10), the macroscopic fading for RIS-link can be written as

$$\text{MF}_{\text{ris,RISFSPL}} = \frac{P_t}{P_r} = \frac{64\pi^3 (d_t d_r)^2}{G_t \lambda^2 LA}. \tag{11}$$

The macroscopic fading for the direct link $\text{MF}_{\text{d,RISFSPL}}$ can be obtained from existing pathloss models, such as the free space pathloss model and pathloss models from the 3GPP standard. The path gain of the direct link and RIS-link can be expressed as β_d and β_{ris}, respectively. $\beta_d = 1/\sqrt{\text{MF}_{\text{d,RISFSPL}}}$ and $\beta_{\text{ris}} = 1/\sqrt{\text{MF}_{\text{ris,RISFSPL}}}$.

Then the total channel can be calculated as

$$h_{\text{tot}} = \beta_d h_d + \beta_{\text{ris}} h_{\text{ris}}, \tag{12}$$

where

$$h_{\text{ris}} = \frac{1}{\sqrt{L}} \mathbf{h}_r \Phi \mathbf{h}_t^{\text{H}}, \tag{13}$$

and $\Phi = \text{diag}(e^{j\phi^{(1)}}, ..., e^{j\phi^{(L)}})$ represents the phase shifts of the RIS. In (13) we normalize h_{ris} by $1/\sqrt{L}$ to compensate for the factor L in (11), because the effect of L is already included in the multiplication of $\mathbf{h}_r \Phi \mathbf{h}_t^{\text{H}}$.

Now we extend to a complex scenario that contains W single-antenna BSs, U single-antenna users, and G RISs. The g-th RIS consists of L_g elements with the diagonal phase shifts matrix Φ_g, and each element has the effective size of A_g. The total channel for the u-th user and the w-th BS can be written as

$$h_{u,w} = \beta_{u,w}^{(d)} h_{u,w}^{(d)} + \sum_{g=1}^{G} \beta_{u,g,w}^{(\text{ris})} h_{u,g,w}^{(\text{ris})}, \tag{14}$$

where $\beta_{u,w}^{(d)}$ and $h_{u,w}^{(d)}$ are the macroscopic fading and small-scale fading for the u-th user and the w-th BS, respectively. Whereas $\beta_{u,g,w}^{(\text{ris})}$ and $h_{u,g,w}^{(\text{ris})}$ are the macroscopic and small-scale fadings for the link of the u-th user, g-th RIS, and the w-th BS, respectively. $h_{u,g,w}^{(\text{ris})} = \frac{1}{\sqrt{L_g}} \mathbf{h}_{u,g} \Phi_g \mathbf{h}_{g,w}^{\text{H}}$ with $\mathbf{h}_{u,g} \in \mathbb{C}^{1\times L_g}$ the channel between the u-th user and the g-th RIS, and $\mathbf{h}_{g,w} \in \mathbb{C}^{1\times L_g}$ the channel between the g-th RIS and the w-th BS. $\beta_{u,g,w}^{(\text{ris})} = \sqrt{\frac{G_w \lambda^2 L_g A_g}{64\pi^3 (d_{g,w} d_{u,g})^2}}$ with $d_{g,w}$ the distance between the g-th RIS and the w-th BS, and $d_{u,g}$ the distance between the u-th user and the g-th RIS. The antenna gain of the w-th BS is G_w.

B. Ray Tracing (RT) Model

The RISFSPL model required LOS conditions and cannot model the pathloss in a realistic environment that includes 3D buildings, blockages, streets, etc. Therefore, we use the MATLAB ray tracer to obtain a more precise macroscopic fading. Both the SLS and the MATLAB ray tracer support open street map scenarios. Hence, we can simulate the same scenarios, i.e., the same building, street, environment, and locations of BSs, RISs, and users in the ray tracer and the SLS.

The MATLAB ray tracer generates LOS and reflection rays between each network node. We use the same scenario described in Sec. II-A: one single-antenna BS and user, and one RIS with L elements. In the SLS, the macroscopic fading for the RIS-link from the ray tracer is calculated as

$$\tilde{\text{MF}}_{\text{ris,RT}} = \frac{1}{G_t} \tilde{\text{PL}}_{ur} \tilde{\text{PL}}_{rb}, \tag{15}$$

where $\tilde{\text{PL}}_{ur}$ and $\tilde{\text{PL}}_{rb}$ are pathloss of the RIS-user and BS-RIS links, respectively. Assuming there is only one LOS path between the RIS and user, and one LOS path between the BS and the RIS, the pathloss of the two links are obtained by

$$\tilde{\text{PL}}_{ur} = (4\pi d_{ur}/\lambda)^2, \tag{16}$$

and

$$\tilde{\text{PL}}_{rb} = (4\pi d_{rb}/\lambda)^2, \tag{17}$$

with d_{ur} and d_{rb} the propagation distances of these links. Hence, (15) becomes

$$\tilde{\text{MF}}_{\text{ris,RT}} = \frac{(4\pi)^4 (d_{ur} d_{rb})^2}{G_t \lambda^4}. \tag{18}$$

However, this macroscopic fading does not include the RIS effect. When the RIS size or element number changes, the macroscopic fading is the same, which is incorrect. Therefore, this pathloss model needs to be modified.

Through comparison between the (18) and (11), we introduce a RIS size factor $\eta = \lambda^2/4\pi LA$ and multiply it with (18), we will get the same results as in (11). The modified macroscopic fading for RIS-link from the RT is obtained by

$$\text{MF}_{\text{ris,RT}} = \eta \tilde{\text{MF}}_{\text{ris,RT}} = \frac{\eta}{G_t} \tilde{\text{PL}}_{ur} \tilde{\text{PL}}_{rb}, \tag{19}$$

Now we consider a normal scenario in the ray tracer where there are K, N, and M paths (including both LOS and non-line-of-sight (NLOS)) for the BS-user, RIS-user, and BS-RIS links, respectively. The indices $(\cdot)_{ub}^{(k)}$, $(\cdot)_{ur}^{(n)}$, and $(\cdot)_{rb}^{(m)}$ denote the variables over the k-th path between the BS and the user, variables over the n-th path between the RIS and the user, and variables over the m-th path between the BS and the RIS,

respectively. Since the pathloss is obtained by each ray from the ray tracer, we cannot directly obtain the overall pathloss for each link. However, we can calculate the overall received power for each link.

First, the received power for the BS-user, RIS-user, and BS-RIS links are calculated as

$$P_{ub} = \left| \sum_{k=1}^{K} \left(\sqrt{P_t / \mathrm{PL}_{ub}^{(k)}} \exp(-j\vartheta_{ub}^{(k)}) \right) \right|^2, \tag{20}$$

$$P_{ur} = \left| \sum_{n=1}^{N} \left(\sqrt{P_{\mathrm{ris}} / \mathrm{PL}_{ur}^{(n)}} \exp(-j\vartheta_{ur}^{(n)}) \right) \right|^2, \tag{21}$$

and

$$P_{rb} = \left| \sum_{m=1}^{M} \left(\sqrt{P_t / \mathrm{PL}_{rb}^{(m)}} \exp(-j\vartheta_{rb}^{(m)}) \right) \right|^2. \tag{22}$$

In these equations, $\mathrm{PL}_{ub}^{(k)}$, $\mathrm{PL}_{ur}^{(n)}$, and $\mathrm{PL}_{rb}^{(m)}$ are the pathloss of the specific propagation path obtained from the same way as (16) and (17). The terms $\vartheta_{ub}^{(k)}$, $\vartheta_{ur}^{(n)}$, and $\vartheta_{rb}^{(m)}$ denote the propagation phases of these links. P_{ris} is the transmit power from the RIS, which is assumed the same as the received signal power at that RIS.

Next, we calculate the overall pathloss for these links as

$$\mathrm{PL}_{ub} = P_t / P_{ub}, \tag{23}$$

$$\mathrm{PL}_{ur} = P_{\mathrm{ris}} / P_{ur}, \tag{24}$$

and

$$\mathrm{PL}_{rb} = P_t / P_{rb}. \tag{25}$$

Finally, in a general scenario where each link consists of multiple reflection paths, we replace the $\tilde{\mathrm{PL}}_{ur}$ and $\tilde{\mathrm{PL}}_{rb}$ in (19) with PL_{ur} and PL_{rb} in (24) and (25), then we get the final macroscopic fading for the RIS-link as

$$\mathrm{MF}_{\mathrm{ris,RT}} = \frac{\eta}{G_t} \mathrm{PL}_{ur} \mathrm{PL}_{rb}, \tag{26}$$

The macroscopic fading for the direct link from the RT is obtained as

$$\mathrm{MF}_{\mathrm{d,RT}} = \frac{1}{G_t} \mathrm{PL}_{ub}. \tag{27}$$

After acquiring the macroscopic fading, we follow the same steps as in Sec. II-A, to calculate the small-scale fading and so on. The path gain of the direct and RIS-link become $\beta_d = 1/\sqrt{\mathrm{MF}_{\mathrm{d,RT}}}$ and $\beta_{\mathrm{ris}} = 1/\sqrt{\mathrm{MF}_{\mathrm{ris,RT}}}$, respectively.

III. Verification in a SISO scenario

To verify the implemented RISFSPL and RT model, we conduct Monte Carlo simulations in a simple SISO scenario with a strong LOS component for which we expect both models to show very similar results. We download a region in Vienna from the OpenStreetMap, and place one single-antenna BS, one single-antenna user, and a RIS with L elements in the scenario as shown in Fig. 1. The BS, RIS, and user heights are 30 m, 20 m, and 1.5 m, respectively. Since RIS mainly contributes to blocked users, we set the macroscopic fading for the direct link as $\mathrm{MF}_d = 200\ dB$ to assume the direct link is blocked so that we only observe the contribution caused by RIS. The center frequency is 3.5 GHz, and the bandwidth is 20 MHz for the simulation.

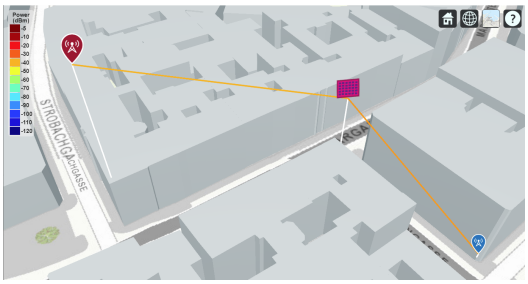

Figure 1. A SISO simulation scenario (the red, pink, and blue icons represent BS, RIS, and user, respectively).

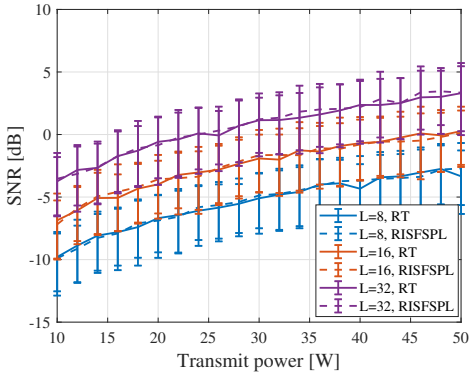

Figure 2. SNR results with random RIS phase shifts.

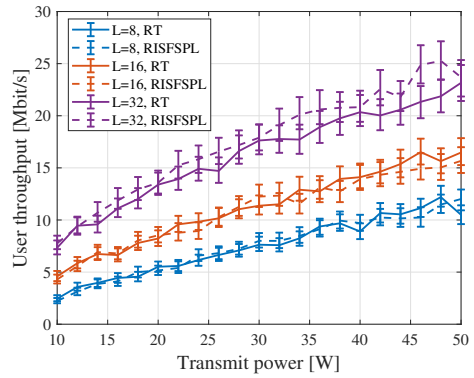

Figure 3. Throughput results with random RIS phase shifts.

The resulting curves in this section are plotted with a 95% confidence interval, revealing that after running a large number of independent simulations, 95% of values will fall into this range. The simulation results of SNR with random RIS phase shifts are shown in Fig. 2. In principle, when we double the RIS element number L, the SNR should grow 3 dB according to the power scaling law [16] because the RIS phase shifts are random. In this figure, the SNR from the SLS shows consistent results with the power scaling law, where 3 dB gain can be observed when we double the RIS element L from 8 to 16 and to 32. In addition, the results from the RISFSPL and RT models are almost identical, which verifies that the RIS size

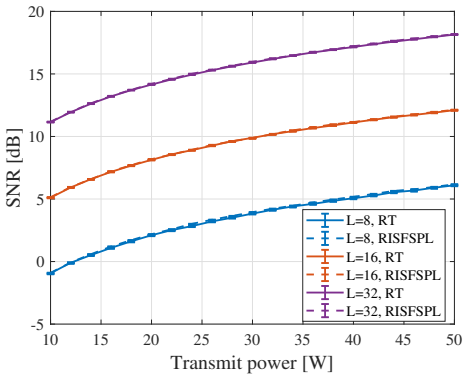

Figure 4. SNR results with optimized RIS phase shifts.

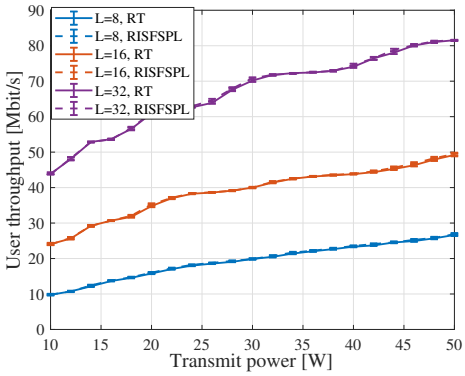

Figure 5. Throughput results with optimized RIS phase shifts.

factor η leads to the equivalent results from the RISFSPL and RT models.

The throughput results with random RIS phase shifts are shown in Fig. 3. The results from the RISFSPL and RT models also show good consistency. The throughput is improved when increasing L. Fig. 4 and Fig. 5 show the results of SNR and throughput with optimized RIS phase shifts, respectively. From Fig. 4, we can observe that the SNR grows 6 dB when doubling L for both the RISFSPL and RT models. The throughput improves with the increasing L. Both the SNR and throughput results are much better than the results with random RIS phase shifts. The results from the RISFSPL and RT models are consistent in these figures, too.

In conclusion, the simulation in such a SISO scenario verifies our implementation of RIS in the Vienna SLS. For more complex scenarios, we can use the modified RT model to replace the RISFSPL model for more precise results. For example, the RT model can also include other effects such as penetration loss through different buildings, effects of different materials and reflecting surfaces, etc.

IV. Simulation in a Complex Scenario

After verification of the RIS module in the SLS, we can conduct simulations in more complex scenarios. Fig. 6 shows an example of a complex scenario with RIS. In this scenario, the environment and heights of BSs, users, and RISs are the same as in Fig. 1, except that in this scenario, there are two BSs, 15 RISs, and many users randomly located on the street. Similarly, to only observe the influence of RIS-assisted links,

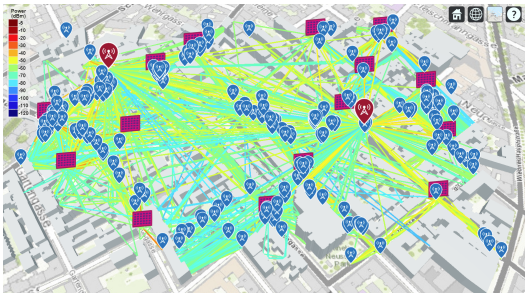

Figure 6. A complex simulation scenario.

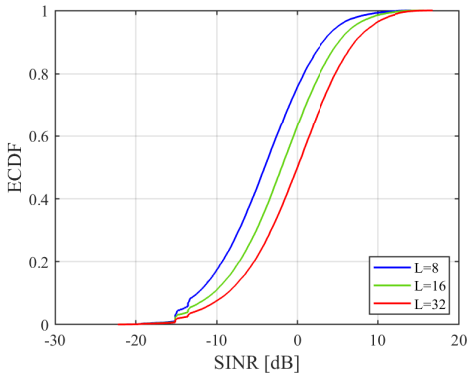

Figure 7. SINR results with random RIS phase shifts.

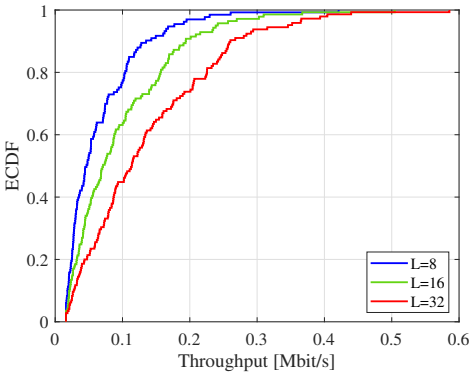

Figure 8. Throughput results with random RIS phase shifts.

we set the pathloss for all direct links as 200 dB, assuming that the direct links are all blocked. The RIS-assisted links obtain the pathloss from the modified RT model.

Next, we compare the simulation results in the scenarios with random and optimized RIS phase shifts. In the former case, all RIS phase shifts are random variables. In the latter case, for each associated user-BS pair, we find the RIS that leads to the highest received power at the user, then that RIS is the desired RIS for that user-BS pair. The received power is only based on the macroscopic fading, and the small-scale fading is not involved. Hence, the RIS with the shortest propagation path is usually the desired RIS for the user. Next, we optimize the phase shifts of this desired RIS and other RISs remaining random phase shifts for this user.

The results of SINR with random RIS phase shifts are shown in Fig. 7. From this figure, we can find that with increased L, the empirical cumulative distribution function (ECDF) of the SINR gets improved. A similar trend can be

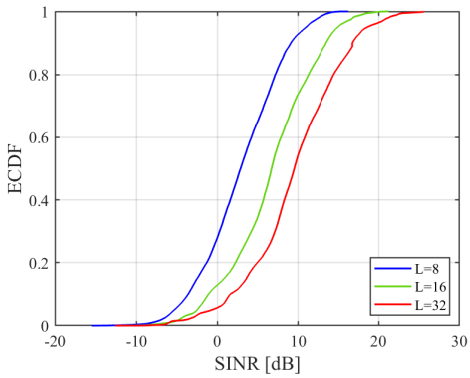

Figure 9. SINR results with optimized RIS phase shifts.

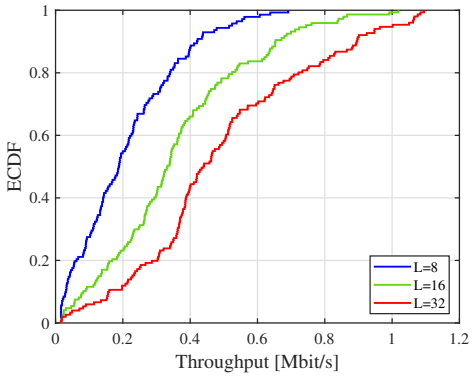

Figure 10. Throughput results with optimized RIS phase shifts.

discovered in Fig. 8 for the throughput. The throughput results get better when L is increased. The maximum throughput value is higher when L is larger.

The SINR and throughput with optimized phase shifts are shown in Fig. 9 and Fig. 10, respectively. Compared with the results from random phase shifts, the optimized phase shifts lead to much higher SINR and throughput. When increasing L, the SINR and throughput are both improved. The range of SINR and throughput values in the case of optimized RIS phase shifts are higher than the results with random phase shifts. For example, when we observe the results with $L = 32$, the maximum SINR reaches 26 dB with optimized RIS phase shifts, whereas the maximum SINR is 17 dB with random phase shifts. The maximum throughput with optimized RIS phase is 1.1 Mbit/s, while the random phase shifts lead to around 0.6 Mbit/s.

V. Conclusion

This paper first introduces the RIS-tailored Vienna SLS integrated with the MATLAB ray tracer. A recently published free space pathloss model for RIS has been adopted in the simulator. However, the original RISFSPL model cannot model the pathloss in a realistic 3D environment, and the original RT model does not include the effect of RIS. Hence, we modified both models and validated them via simulations in a simple SISO scenario in the SLS. Results demonstrate that the modified RT model achieves the same impact as the modified RISFSPL model. Therefore, the modified RT model includes advantages from both models. Next, we use the modified RT model to replace the RISFSPL model for more complex scenarios. We conducted system-level simulations in a complex scenario consisting of multiple BSs, users, and RISs. The results show apparent improvements with optimized RIS phase shifts than random phase shifts.

Acknowledgment

This work is fully funded by the European Union's Horizon 2020 research and innovation programme under the Marie Skłodowska-Curie grant agreement No 956256.

References

[1] M. A. ElMossallamy, H. Zhang, L. Song, K. G. Seddik, Z. Han, and G. Y. Li, "Reconfigurable intelligent surfaces for wireless communications: Principles, challenges, and opportunities," May 2020.

[2] Q. Wu, S. Zhang, B. Zheng, C. You, and R. Zhang, "Intelligent reflecting surface-aided wireless communications: A tutorial," vol. 69, pp. 3313–3351, 2021.

[3] T. Zhou, K. Xu, X. Xia, W. Xie, and J. Xu, "Achievable Rate Optimization for Aerial Intelligent Reflecting Surface-Aided Cell-Free Massive MIMO System," vol. 9, pp. 3828–3837, 2021.

[4] M. Najafi, V. Jamali, R. Schober, and H. V. Poor, "Physics-based modeling and scalable optimization of large intelligent reflecting surfaces," vol. 69, pp. 2673–2691, 2021.

[5] M. Di Renzo, A. Zappone, M. Debbah, M.-S. Alouini, C. Yuen, J. de Rosny, and S. Tretyakov, "Smart radio environments empowered by reconfigurable intelligent surfaces: How it works, state of research, and the road ahead," *IEEE Journal on Selected Areas in Communications*, vol. 38, no. 11, pp. 2450–2525, 2020.

[6] M. Di Renzo, F. H. Danufane, and S. Tretyakov, "Communication models for reconfigurable intelligent surfaces: From surface electromagnetics to wireless networks optimization," *Proceedings of the IEEE*, vol. 110, no. 9, pp. 1164–1209, 2022.

[7] C. Huang, A. Zappone, G. C. Alexandropoulos, M. Debbah, and C. Yuen, "Reconfigurable intelligent surfaces for energy efficiency in wireless communication," *IEEE Transactions on Wireless Communications*, vol. 18, no. 8, pp. 4157–4170, 2019.

[8] J. Jeong, J. H. Oh, S. Y. Lee, Y. Park, and S.-H. Wi, "An improved pathloss model for reconfigurable-intelligent-surface-aided wireless communications and experimental validation," *IEEE Access*, vol. 10, pp. 98065–98078, 2022.

[9] B. Sihlbom, M. I. Poulakis, and M. D. Renzo, "Reconfigurable intelligent surfaces: Performance assessment through a system-level simulator," *IEEE Wireless Communications*, pp. 1–10, 2022.

[10] "https://www.tuwien.at/etit/tc/en/vienna-simulators/vienna-5g-simulators/."

[11] W. Tang, M. Z. Chen, X. Chen, J. Y. Dai, Y. Han, M. Di Renzo, Y. Zeng, S. Jin, Q. Cheng, and T. J. Cui, "Wireless communications with reconfigurable intelligent surface: Path loss modeling and experimental measurement," *IEEE Transactions on Wireless Communications*, vol. 20, no. 1, pp. 421–439, 2021.

[12] L. Hao, A. Fastenbauer, S. Schwarz, and M. Rupp, "Towards system level simulation of reconfigurable intelligent surfaces," in *2022 International Symposium ELMAR*, pp. 81–84, 2022.

[13] W. Tang, J. Y. Dai, M. Z. Chen, K. Wong, X. Li, X. Zhao, S. Jin, Q. Cheng, and T. J. Cui, "Design and implementation of MIMO transmission through reconfigurable intelligent surface," in *21st IEEE International Workshop on Signal Processing Advances in Wireless Communications, SPAWC 2020, Atlanta, GA, USA, May 26-29, 2020*, pp. 1–5, IEEE, 2020.

[14] S. R. Saunders and A. Aragón-Zavala, *Antennas and propagation for wireless communication systems*. Chichester, England: J. Wiley & Sons, 2nd ed., 2007.

[15] B. Tahir, S. Schwarz, and M. Rupp, "Analysis of Uplink IRS-Assisted NOMA Under Nakagami-m Fading via Moments Matching," *IEEE Wireless Communications Letters*, vol. 10, no. 3, pp. 624–628, 2021.

[16] K. Zhi, C. Pan, H. Ren, and K. Wang, "Power Scaling Law Analysis and Phase Shift Optimization of RIS-Aided Massive MIMO Systems With Statistical CSI," *IEEE Transactions on Communications*, vol. 70, no. 5, pp. 3558–3574, 2022.